



# Investigation of forging performance for AA6082

Ozkan Tunc<sup>1</sup> · Ilyas Kacar<sup>2</sup> · Fahrettin Ozturk<sup>3,4</sup>

Received: 26 February 2021 / Accepted: 12 July 2021 / Published online: 10 August 2021  
© The Author(s), under exclusive licence to Springer-Verlag London Ltd., part of Springer Nature 2021

## Abstract

6XXX series aluminum alloys are generally excellent alternatives to steels for many forged parts in aerospace and automotive industries. In this study, the forging performance of the 6082 aluminum alloy is investigated in order to replace the existing material for forged steel parts. The effect of artificial aging of the alloy on the microstructure and mechanical properties is studied. Optimum aging conditions are determined. Results reveal that AA6082 could be a good replacement for applications where shock and vibrational loads exist. The rod end automotive part currently manufactured from AISI1045 can be replaced by AA6082 without any design changes. The major drawback is that the cold forging of the aged alloy is poor due to its brittle nature and crack initiations. Therefore, warm or hot forging is recommended to overcome the poor forgeability.

**Keywords** Al-Si alloy · AA6082 · Artificial aging · Hot forging · Fatigue · Automotive

## 1 Introduction

Reducing the fuel consumption and carbon dioxide emissions is a challenging issue in automotive industry. Design changes and using lighter materials are some strategies used by the car part manufacturers. 6082 aluminum alloy (AA6082) is a good candidate as an alternative material, because it is lighter than steel and it is abundantly available among other aluminum alloys. Mechanical properties improved by aging process are comparable to the steels. Therefore, this alloy has the potential to be a good replacement for steel parts in the suspension, chassis, and engine. For example, in the aviation industry, the arms in the flight control mechanism and the brake bodies are often made of AA6082. However, due to the strict regulations in the aerospace and automotive industry, it is a problematic situation to determine whether a one-to-one replacement with the use of a new material is possible

without changing the design of the part. A change in design can irrevocably lead to additional development time, process, and expertise costs for the manufacturers since the part needs to meet the same set of requirements. It is well-known that the trial and error method is not a cost-effective method. Also an inverse engineering is often not possible since the applications are unique. Whether thermo-mechanical treatments can solve this problem is the primary scope of this study.

Aging is a time- and temperature-dependent heat treatment process. AA6082 is one of the suitable materials for artificial aging. Different aging conditions lead to different mechanical properties. AA6082 is often artificial aged at 160 °C, after dissolving at 500 °C [1]. While the tensile strength of AA6082-O which is a not heat-treated alloy is around 170 MPa, it can reach 427 MPa after aging [2]. However, the microstructure becomes brittle, and its impact energy absorption ability decreases. On the other hand, the strength suffers when the forgeability increases [3]. It has been reported that both strength and forgeability decrease in the absence of dissolving [4]. Thus, a careful aging process design is needed to attain both high strength and high toughness together.

The forgeability of AA6082 is poor for cold forging due to crack initiations [5]. The forgeability increases at elevated temperatures up to 160 °C [6]. The forgeability can increase up to 159% with warm forging [7]. Grain recovery affects the deformability [8]. The process temperature of the hot forging acts as a dissolving process. The artificial aging after the hot forging leads to a homogeneous grain distribution in the

✉ Ilyas Kacar  
ikacar@ohu.edu.tr

<sup>1</sup> Ditas Dogan Yedek Parca Imalat and Teknik A.S., Nigde, Turkey

<sup>2</sup> Mechatronics Engineering Department, Nigde Omer Halisdemir University, Nigde, Turkey

<sup>3</sup> Mechanical Engineering Department, Ankara Yildirim Beyazıt University, Ankara, Turkey

<sup>4</sup> Turkish Aerospace Industries, Inc., Ankara, Turkey

microstructure [9]. When hot billets without extrusion are forged directly, a homogeneous microstructure and a more economical forging are guaranteed [10].

The forgeability increases by increasing soaking duration due to the homogeneous distribution of the phases inside the microstructure at the dissolution stage [11–13]. A 15-min waiting time at 540 °C is suggested for dissolution [14]. Water is frequently used as a cooling medium. Fast cooling ensures the smaller-sized Mg<sub>2</sub>Si solid precipitates in the microstructure. Finer or distorted precipitates can cause the strength increase [15, 16]. The β''-(Mg<sub>5</sub>Si<sub>6</sub>) phase seen up to 300 °C is the main factor in the strength increment. When it transforms into β'-(Mg<sub>1.8</sub>Si) and β-(Mg<sub>2</sub>Si), the strength decreases. Increasing number of the solid precipitates in the microstructure makes the material more brittle [17]. The β'' phase is rich in dislocations [18, 19]. Increasing temperature decreases the number of dislocations [20].

The hardening behavior of the alloy is clearly seen during successive forgings [21]. It is important to create plastic deformation in simulations. The alloy is sensitive to deformation rate during forging, and its tensile strength increases at high strain rates [17].

AA6082 alloy presents high flexibility in terms of mechanical properties depending on the heat treatment and deformation conditions. The novelty of the work is that the optimum heat treatment conditions have been investigated to replace the material of the automotive rod end part. The part was manufactured by hot forging for AISI1045 steel, meanwhile AA6082-O (ISO: AlSi1MgMn) alloy has been investigated as a replacement of it. Replacing a structural part with the lighter one without sacrificing safety, manufacturing time, and economy is of primary concern for the car part manufacturers. The effect of aging on the microstructure was also presented. Optimum values were used in fatigue and hot forging simulations. Press force requirement for forging, the burr ratio, the processing time, the residual stress, the deformation, and the service life of the rod end were compared.

## 2 Materials and experiments

Extruded rods with a 20-mm diameter were used for sample preparation. The compositions of AA6082-O and AISI1045

are given in Table 1. The chemical compositions are critical for the required heat treatment, the material microstructure, and the mechanical properties of the materials.

### 2.1 Heating and cooling sequences

Heating temperature and duration, types of quenching medium, sequential treatments, and soaking time were investigated. The alloy was heated up to the dissolution temperature at a heating rate of 36 °C/s. When the temperature reached the set value, the samples were kept for 2–10 h inside the furnace. Then the samples were air cooled or quenched in water or water-polymer mixtures. The mixtures contained 25% polymer, 50% polymer, and 75% polymer, respectively. The dissolved samples were then artificially aged at 175–220 °C during 2–10 h. The artificial aging process was also repeated sequentially for some samples. A scheme of the aging treatment is shown in Fig. 1. Quenching environments composed of 1%, 2%, 3%, 4%, 5%, 6%, 7%, and 8% polymer-water mixtures were also investigated to determine their effects on the mechanical properties.

The specimen designation for tests is summarized in Table 2. It also gives their ultimate tensile strength (UTS) and strain at break.

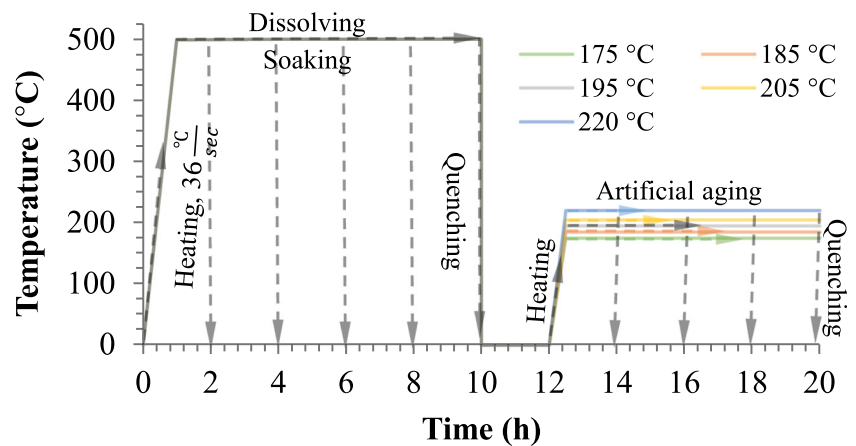
### 2.2 Testing procedures for tensile strength, fatigue strength, impact resistance, and hardness

A Shimadzu Autograph 100 kN testing machine with a video type extensometer system was used to perform the tensile tests. The monotonic tension curve (strain  $\epsilon$  and stress  $\sigma$ ) was constructed in the linear coordinate system by using specimens prepared following the ASTM B557 M 02A standard [22] as seen in Fig. 2a. The tensile test specimens have a 50-mm initial gauge length. A 0.0083 s<sup>-1</sup> (25 mm/min) strain rate was applied in the tensile test for the aged specimens, while 0.0003, 0.0083, and 0.033 s<sup>-1</sup> were used for determination of the strain rate sensitivity parameters in the jump test. Figure 2b and c show the dimensions of the fatigue and impact test specimens prepared according to ASTM E606-92 [23] and ISO 148-1 [24], respectively. Fatigue tests were conducted at a constant frequency of 1 Hz, the load was fully reversed, and the amplitude was kept constant to provide a zero mean stress. Since there is no endurance limit for nonferrous

**Table 1** Chemical compositions of AA6082 and AISI1045 (wt.%)

AISI 1045	C	Si	Mn	P	Cu	Cr	Mo	Ni	Al	S	Sn
	0.44	0.26	0.65	0.007	0.18	0.15	0.04	0.04	0.02	0.03	0.015
AA 6082	Mg	Si	Mn	Fe	Cu	Cr	Ti	Ni	Al	Zn	Co
	0.99	3.54	1.84	1.44	3.76	1.39	0.68	2.38	72.69	2.62	1.96

**Fig. 1** A scheme for the heat treatment cycle



materials, the data were collected after 1 million cycles for AA6082.

Hardness measurements were carried out according to the ASTM E92 [25] standard by applying a 5-kg load for 15 s using the Vickers hardness measurement method. The hardness reading regions on the specimens are given in Fig. 3.

### 2.3 Microstructural investigation

Before microstructural investigation, the specimens were placed inside an epoxy filling material for cold molding. They were grinded, polished, and etched, respectively. For these procedures, a Struers Labopol-5 automatic polishing unit was used. Sandpapers in the order of 320, 500, 1200, 2400, and 4000 grids were used successively for grinding. Specimens were cooled with pure water during the grinding process to prevent any microstructural change. Diamond suspensions in the different grain sizes and corresponding polishing fabrics were used in the polishing process. The finer grains lead to the fewer surface scratches. A uniform contact between the sample surface and the polishing fabric was confirmed during the polishing process in order to obtain a well-polished specimen surface. Various grain-sized polishing suspensions such as 3  $\mu\text{m}$ , 1  $\mu\text{m}$ , and 0.25  $\mu\text{m}$  and corresponding fabrics have been used. A fabric moisturizer was also sprayed during the polishing to adjust the moisture content. Modified Keller's reagent (2.0 ml HF+98.0 ml H<sub>2</sub>O) was used for etching during a 3-s soaking duration. An Olympus BX-51 optical microscope with  $\times 5$ –100 magnifications was used to take the microstructure images.

### 2.4 Hot forging experiments

A pair of a two-stage hot forging mold was used on a conventional screw press bench as seen in Fig. 4. The forging parameters such as press force, burr ratio, forging time, and mold filling rate were determined experimentally for various

temperatures. The hot forging trials were carried out in the hot forging press workshop of DİTAŞ Inc. [26, 27].

### 2.5 Simulations

Finite element simulations of the hot forging and fatigue were performed. Figure 5 shows a 3D finite element model, its initial conditions, and die-billet geometries for the forging simulations. The parameters such as press force, burr ratio, forging time, mold filling, and temperature were determined from the simulations for various temperatures. Deform 3D© software [28] was used to perform hot forging simulations.

The billet temperature was investigated between 300–525 °C for AA6082 and 750–1250 °C for AISI1045 steel to ensure the hot working conditions. Initial die temperature was 300 °C for both materials. Forging stroke was 50 mm between the dies, while total stroke was 150 mm. The simulations were repeated for 25 °C increments. Since the geometries were non-symmetric, the three-dimensional (3D) model was used.

Tetrahedron elements were used for meshing and automatic re-meshing. While there were 32,670 elements at the beginning, it reached the 100,000 elements approximately due to the re-meshing for converging in the results during simulation. The computing time took 1 h 25 min 20 s by using a workstation computer having 3.70 GHz 16 CPUs, 64 GB RAM, and display device with 8 GB RAM. The outer surfaces of the dies were meshed for getting temperature distributions. The power function given in Eq. (1) [29] was employed as the isotropic hardening rule by combining with the von Mises yield criterion [30] and associated flow rule to set the plasticity model for the cylindrical  $\text{Ø}25 \times 100$ -mm billet material. The die tools were set as rigid bodies.

$$\bar{\sigma} = c \left( \bar{\epsilon} \right)^n \left( \dot{\bar{\epsilon}} \right)^m + y \quad (\text{Eq.1})$$

Here,  $\bar{\sigma}$  is the equivalent stress,  $\epsilon$  is the plastic strain,  $\bar{\epsilon}$  is the equivalent plastic strain, and  $\dot{\bar{\epsilon}}$  is the equivalent plastic strain

**Table 2** The specimen and their tensile results

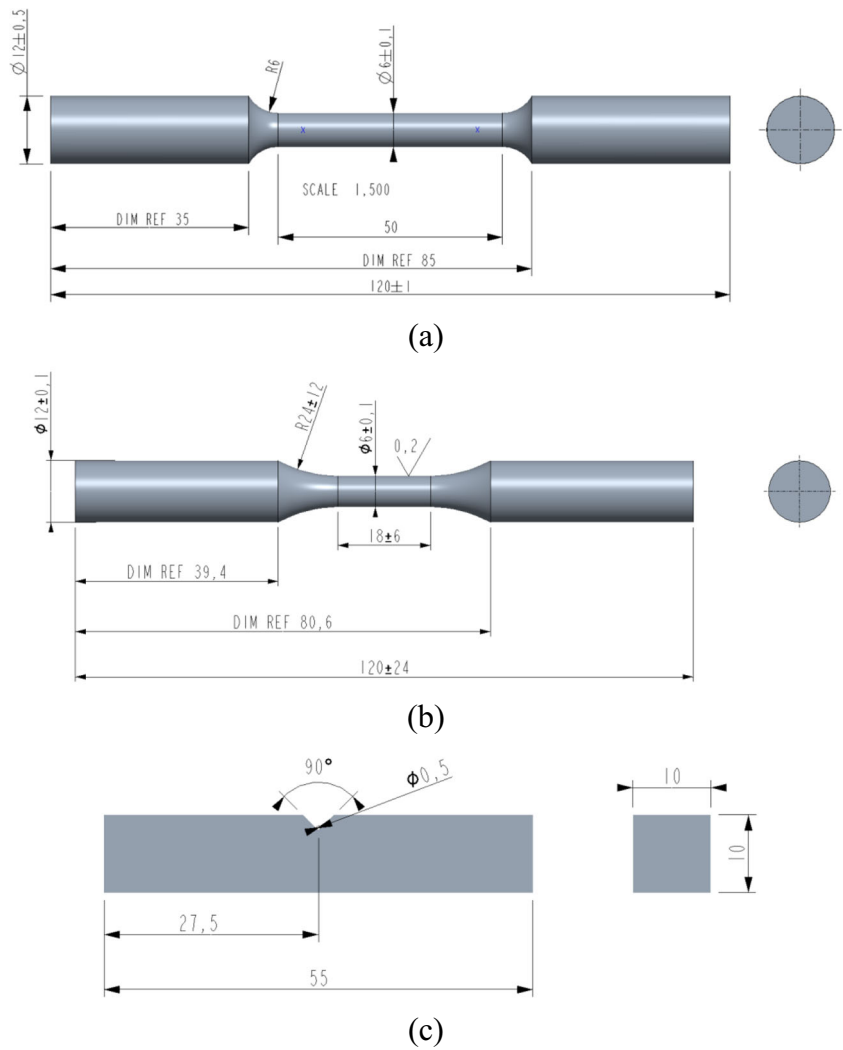
Test no.	Soaking temp. (°C)	Soaking duration (h)	Artificial aging temp. (°C)	Artificial aging duration (h)	Quenching	UTS (MPa)	Strain at break (%)
0 (*)	-	-	-	-	-	166	12.83
1	500	4	-	-	Air	204	9.12
2	500	6	-	-	Air	194	8.37
3	500	8	-	-	Air	218	9.69
4	500	10	-	-	Air	148	9.12
5	500	4	-	-	Water	238	8.16
6	500	6	-	-	Water	244	10.9
7	500	8	-	-	Water	242	10.69
8	500	10	-	-	Water	248	9.91
9	500	2	175	2	Air	218	9.88
10	500	2	175	2	Water	271	8.69
11	500	2	175	2	Water	232	8.79
12	500	2	175	2	%25 polymer	230	8.93
13	500	2	175	2	%50 polymer	217	10.03
14	500	2	185	2	Air	384	8.81
15	500	2	185	4	Water	249	5.96
16	500	2	185	4	%25 polymer	272	7.06
17	500	2	185	4	%50 polymer	273	6.89
18(**)	500	2	185	4	Air	406	7.42
19	500	2	185	6	Air	399	5.25
20	500	2	185	8	Air	391	3.64
21	500	2	185	10	Air	373	4.56
22	545	2	195	2	Water	386	6.89
23	545	2	195	4	Water	391	8.71
24	500	2	195	6	Water	257	7.71
25	500	2	195	6	%25 polymer	265	7.48
26	500	2	195	6	%50 polymer	268	3.90
27	545	2	195	6	Water	365	3.78
28	545	2	195	8	Water	341	3.98
29	545	2	195	10	Water	345	9.67
30	500	2	220	10	Water	156	10.76
31	500	2	220	10	%25 polymer	153	10.12
32	500	2	220	10	%50 polymer	150	10.28
33	500	2	220	10	Air	155	10.56

(\*) AA6082-O was tested for comparison and validation; (\*\*) The sample with the highest UTS

rate,  $y$ ,  $c$ , and  $n$  are the yield point, the plasticity modulus, and the hardening exponent at the room temperature, respectively. While  $c$ ,  $n$ , and  $y$  are determined by curve fitting on the tensile curve,  $m$  is the exponent of the strain rate sensitivity and determined from the jump test curve at the room temperature. At elevated temperatures, they are function of temperature  $T$ , as  $c(T)=199.21e^{-1E-6T}$  (MPa),  $m(T)=0.0037T$ ,  $n(T)=0.009\ln(T)+0.27$ , and  $y(T)=-0.0002T+557.49$  (MPa) for AISI1045 and  $c(T)=-3390\ln(T)+20184$  (MPa),  $m(T)=-0.0091T+7.54$ ,  $n(T)=0.4316\ln(T)-1.99$ , and  $y(T)=-0.162T+117.87$  (MPa) for

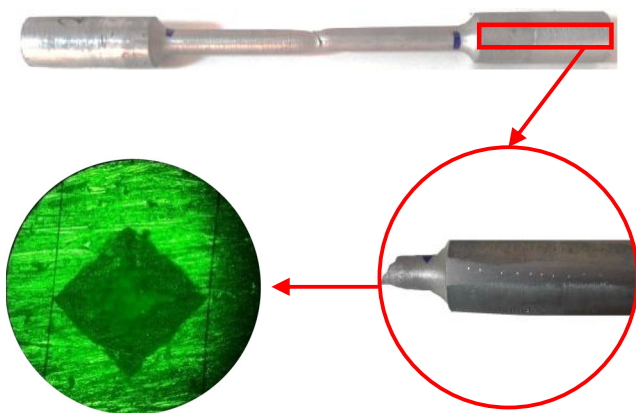
AA6082 whose parameters were calculated from the curves of AA6082-O because the aged alloy turns back to AA6082-O at the hot working temperature. The analysis time interval was set as 1 s and divided into 100 steps. The upper die moved linearly in the vertical direction while the lower one was fixed. In order to avoid waste of time and unnecessary calculations, the upper die was not retracted after forging. The analysis was performed explicitly. Direct solver has been chosen as a solver since it shortens the solution time. The shear friction model was used, and its coefficient at the tool and sample interface

**Fig. 2** Dimensions of **a** tensile, **b** fatigue, and **c** impact test specimens (mm)



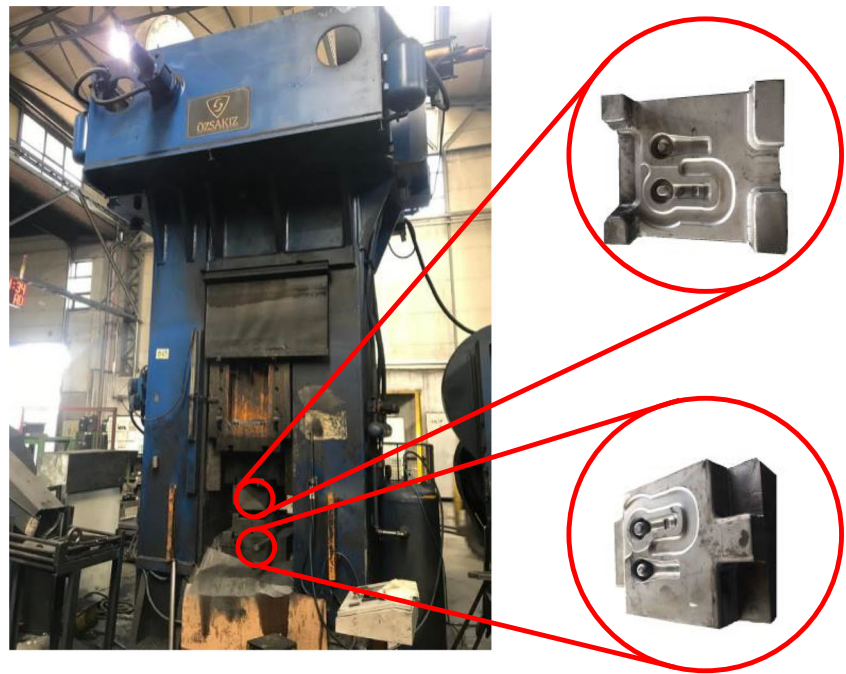
was assumed to be constant and taken as 0.3. The interface heat transfer coefficient between the objects in contact was taken as constant 11 N/sec/mm<sup>2</sup>/°C.

The fatigue simulations were carried out in the strength-life (S-N) type, with a fully reversed loading, and a constant amplitude to ensure the zero mean stress. The Soderberg criterion was chosen as the mean stress correction theory, because of its conservative nature. Material properties in Table 3 for AA6082 and AISI1045 and experimental S-N data were used. Fatigue strength reduction factors  $K_f = 0.634$  for AA6082 and  $K_f = 0.582$  for AISI1045 [31] were used. A finite element model for fatigue analysis is given in Fig. 6. The 3D model was meshed with tetrahedron elements and the solution was performed in a one load step. Totally 1,828,757 elements were used for converging in the results. No re-meshing was applied. To reflect the same boundary conditions in its application area, while the FE model's one end is connected by a fixed support, a 1000-N remote force is applied axially. Two spherical joints on the tie rod and on its own avoid bending loads. Therefore, it carries just axial load. The computing time was 5 min and 39 s for fatigue simulation.



**Fig. 3** The measurement points for hardness

**Fig. 4** Hot forging press and tooling



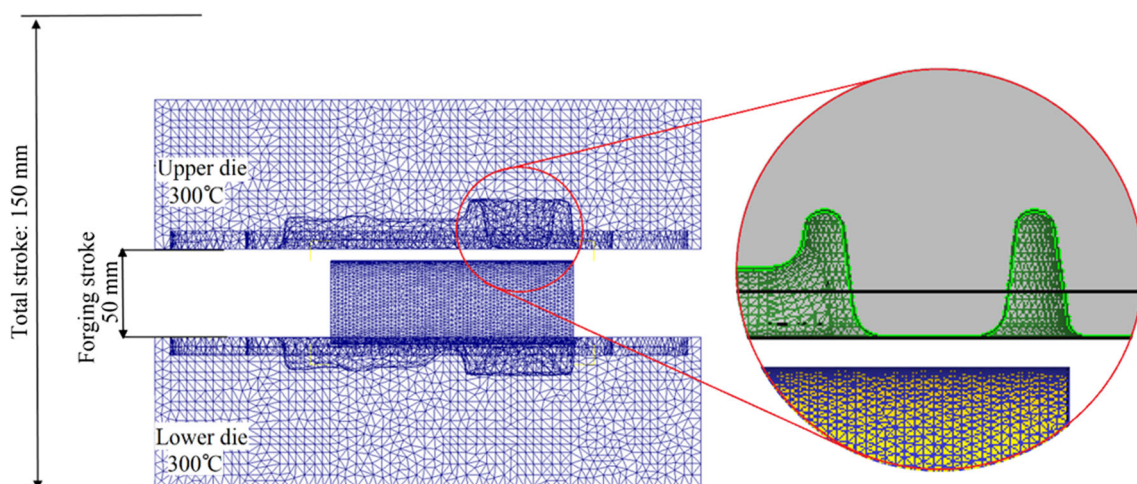
### 3 Results and discussions

#### 3.1 Mechanical properties

UTSs and strains at break for all samples are shown in Fig. 7a and b. The strains of the AA6082 samples were higher than those of the AISI1045 samples. Higher strain means higher formability. Thus, AA6082 has higher formability than AISI1045. The maximum strain is obtained from AA6082-O namely the sample zero where artificial aging is not applied. The aging leads to decrease in formability. Figure 7a indicates that UTSs of AA6082 samples were much lower than those of the AISI1045 sample, which was about 711 MPa. The highest value of AA6082 was 406 MPa.

Engineering stress vs. strain curves of the materials are given in Fig. 8. Although the strength of the AA6082-O samples was quite low, the aged AA6082 sample's strength was improved significantly. It has also higher formability inherently. Yield points of the samples were noticeably distinctive.

Hardness and the Charpy impact tests were also conducted as seen in Fig. 9. It is clear that the hardness of AA6082 increases after all aging treatments. Increased hardness provides more wear resistance but suffers from the toughness. However, the energy-absorbing capability of AA6082 is higher than that of AISI1045. It is also noticed that the hardness decreases from 175 to 122 HV when AA6082 was pre-strained. Some researchers have also shown that the hardness of



**Fig. 5** A finite element model of the hot forging process

**Table 3** Material properties at room temperature

	AISI1045	AA6082-O	AA6082 (*)
Density (gr/cm <sup>3</sup> )	7.85	2.71	2.71
Yield strength (**) (MPa)	415.63	108.91	359.34
Maximum strength (MPa)	651.84	165.33	406

(\*) The specimen 18. (\*\*) Proof strength for AA6082 alloy

aluminum-based alloys has decreased with pre-strain [32–36]. However, steel-based materials have opposite attitude [37–39].

The Wöhler curves were drawn as shown in Fig. 10. While the endurance limit of AISI1045 was 300 MPa, the fatigue strength of AA6082 for more than a million cycles was obtained for the specimen 18 with laboratory-controlled fatigue tests. It is clearly seen no infinite life in AA6082. This is a very well-known issue in aluminum alloys.

### 3.2 Jump test

The strain rate sensitivity coefficient “*m*” to be used in the plasticity equation in the simulations was calculated by using the jump test. The jump test was performed at the room temperature in the tensile test with 0.0003 and 0.033 s<sup>-1</sup> strain rates. A curve was conducted as seen in Fig. 11. The figure also includes the calculation method. The curve includes just

true plastic data. Removing the elastic strain was explained in [40] in detail.

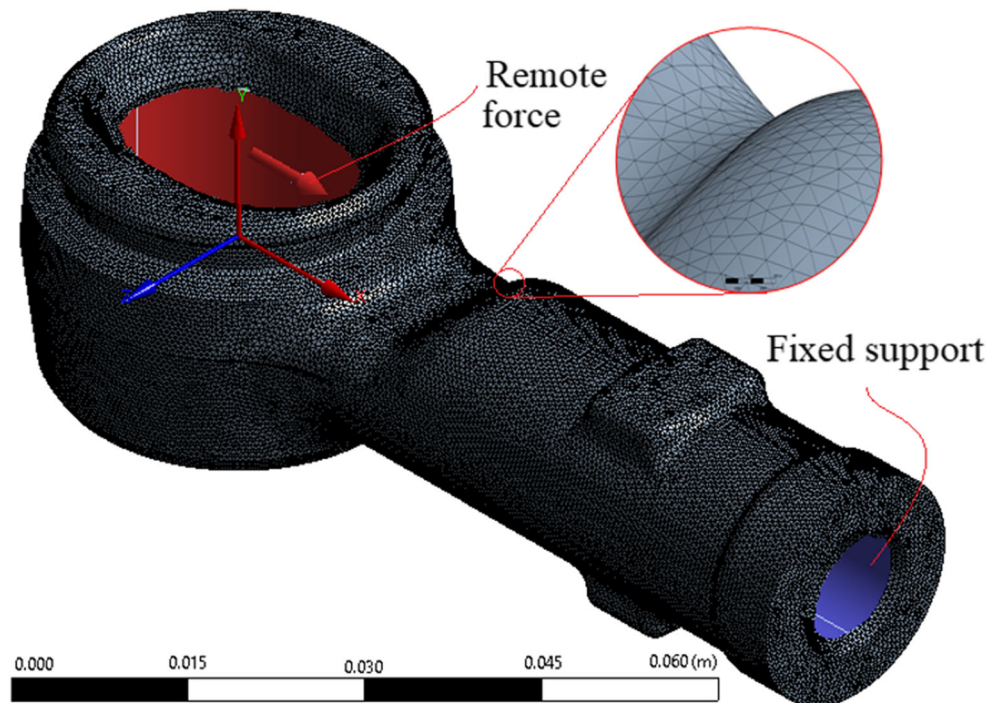
The results are seen in Table 4 where  $\dot{\varepsilon}_1$  and  $\dot{\varepsilon}_2$  are the strain rates before and after a peak, respectively. While  $\sigma_1$  stands for the stress at the beginning of the peak,  $\sigma_j$  is the stress at the peak point.  $\sigma_2$  is the stress at the intersection point of the peak.

### 3.3 Microstructure evaluation

AA6082 basically contains the elements Al, Mg, Si, Ti, Cr, Mn, Fe, Cu, and Zn. The most common intermetallic phase is Mg<sub>2</sub>S. This phase appears as dark regions in the microstructure images. Fe and Mn elements lead to very small amounts of impurities. Fe and Al cause double, triple, and quadruple intermetallic phases such as Al-Fe, Al-Fe-Si, and Al-Fe-Mn-Si. Mn and Cr are elements which balance the Fe content in  $\alpha$ -Al<sub>12</sub>(FeMn)<sub>3</sub>Si or  $\alpha$ -Al<sub>12</sub>(FeCr)<sub>3</sub>Si. The  $\alpha$  phases are detrimental to the mechanical properties.  $\beta$ -Al<sub>3</sub>Fe<sub>2</sub>Si<sub>2</sub> or  $\beta$ -Al<sub>5</sub>FeSi phases contain Fe and Si in the dendritic shape. Intermetallic phases settle in the grain boundary. Microstructure photographs are shown in Fig. 12 where **O**, **□**, **Mg<sub>2</sub>Si**; **Δ**,  $\alpha$ -dendrite; and, freehand drawing for  $\beta$ -dendrite.

Lighter-colored regions in the microstructure images show essential Al elements. As the temperature and artificial aging time increase, the grain size decreases. The amount and size of the dendrites increase with increasing

**Fig. 6** A finite element model for the fatigue simulation



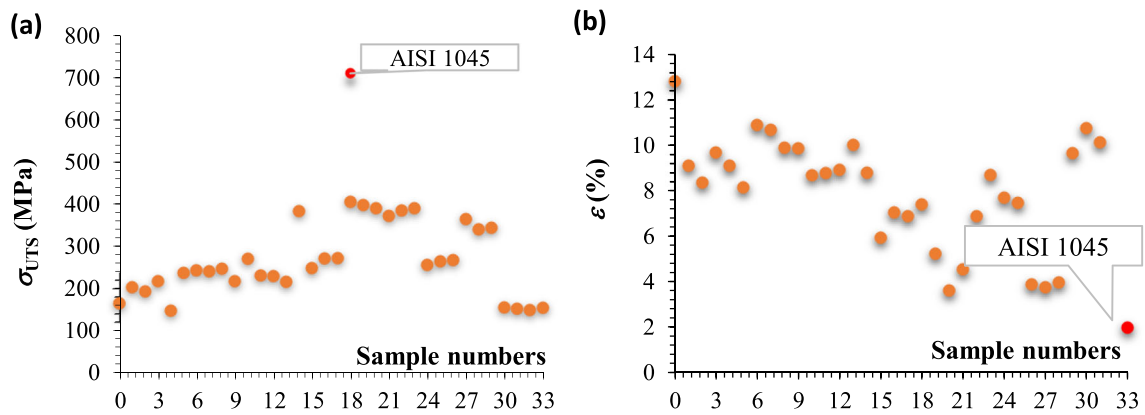


Fig. 7 a UTSs and b strains at break of the AA6082 samples

aging time. Smaller and homogeneous precipitate distribution was obtained by quenching in the 50% polymer + water mixture.

It is observed that the coarse grains are completely dissolved in the microstructure for the samples aged at 175 °C. The  $\beta$ -dendrites have a longer and thicker shape as reported [15, 16]. The micro impurities settled in the grain boundaries lead to an easier movement of the dislocations during deformation. This provides ductility.

When the samples aged at 185 °C were compared to the ones aged at 175 °C, it is seen that the grain size was smaller, which is especially noticeable when the aging time increases. The shape of the  $Mg_2Si$  precipitates becomes smaller and its amount increases. In addition,  $\alpha$ -dendrites and  $\beta$ -dendrites at 185 °C were smaller than those at 175 °C and stayed in the needle-like shapes. The highest UTS was obtained from the sample aged at 185 °C for 4 h. The grains were dissolved in a smaller distribution in samples aged at 195 °C. As the aging time increases, the grain size decreases. The  $Mg_2Si$  phases became smaller and its amount increased. Although the  $\alpha$ -

dendrites and  $\beta$ -dendrites, which are in a needle-like shape, were visible at 185 °C, they became smaller and disappeared in the microstructure at 195 °C.

### 3.4 Hot forging

It is seen that the pressing force requirement decreases at elevated initial billet temperature due to the decreasing yield point. Tables 5 and 6 compare the forging results for AA6082 and AISI1045, respectively. While the die cavity was filled 100% for AISI1045, it was variable for AA6082. In the tables, the burr (%) means its volume fraction with respect to initial billet volume.

The forging process increases the strain energy and the billet temperature, as expected. The temperature variation in the steel was relatively smaller than AA6082. When the initial temperature of the AA6082 billet exceeded 450 °C, the body temperature might reach up to the melting point locally. Melted material cannot fill the die cavity properly and also leads to more burr formation. The temperature change seen during hot forging was more stable for

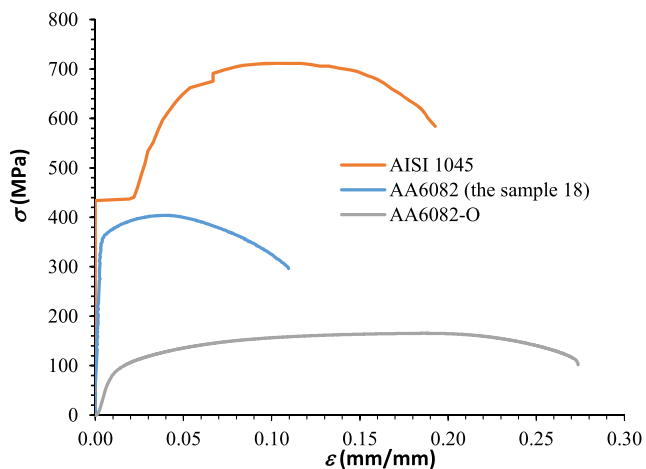


Fig. 8 Comparison of engineering tensile curves of AA6082 and AISI1045

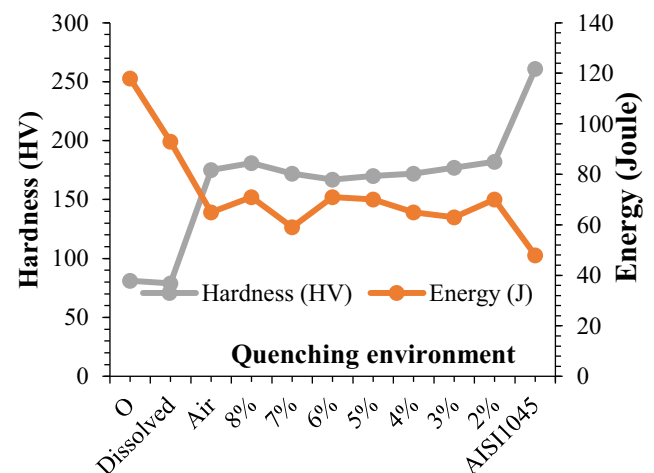
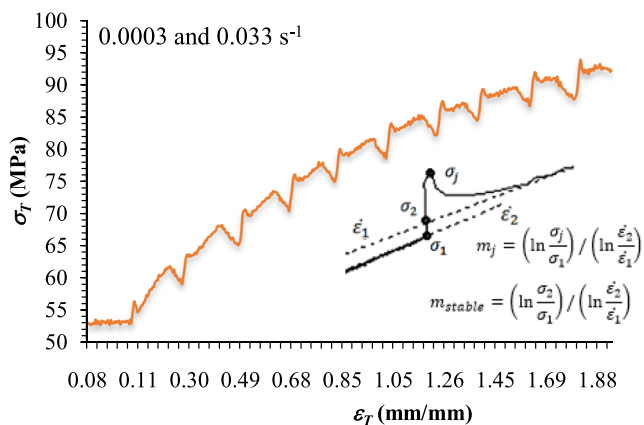
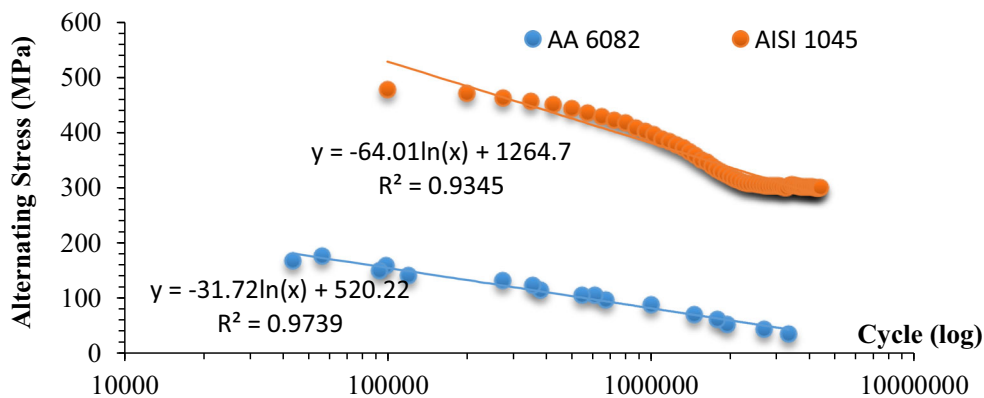


Fig. 9 Hardness and Charpy impact energy



**Fig. 10** Wöhler curves of AISI1045 and the specimen 18



**Fig. 11** Jump test curve

AISI1045. It is concluded that the initial billet temperature must be less than 450 °C.

Validation forgings were performed with various temperatures for AA6082 rod ends as seen in Fig. 13. The amount of burr, the surface condition, and the mold filling ratio can be seen. The mold cavity was not completely filled during forging at higher temperatures than 400 °C. Thus, the increasing amount of burr and the decreasing die filling confirm a good agreement between the simulation and experiments.

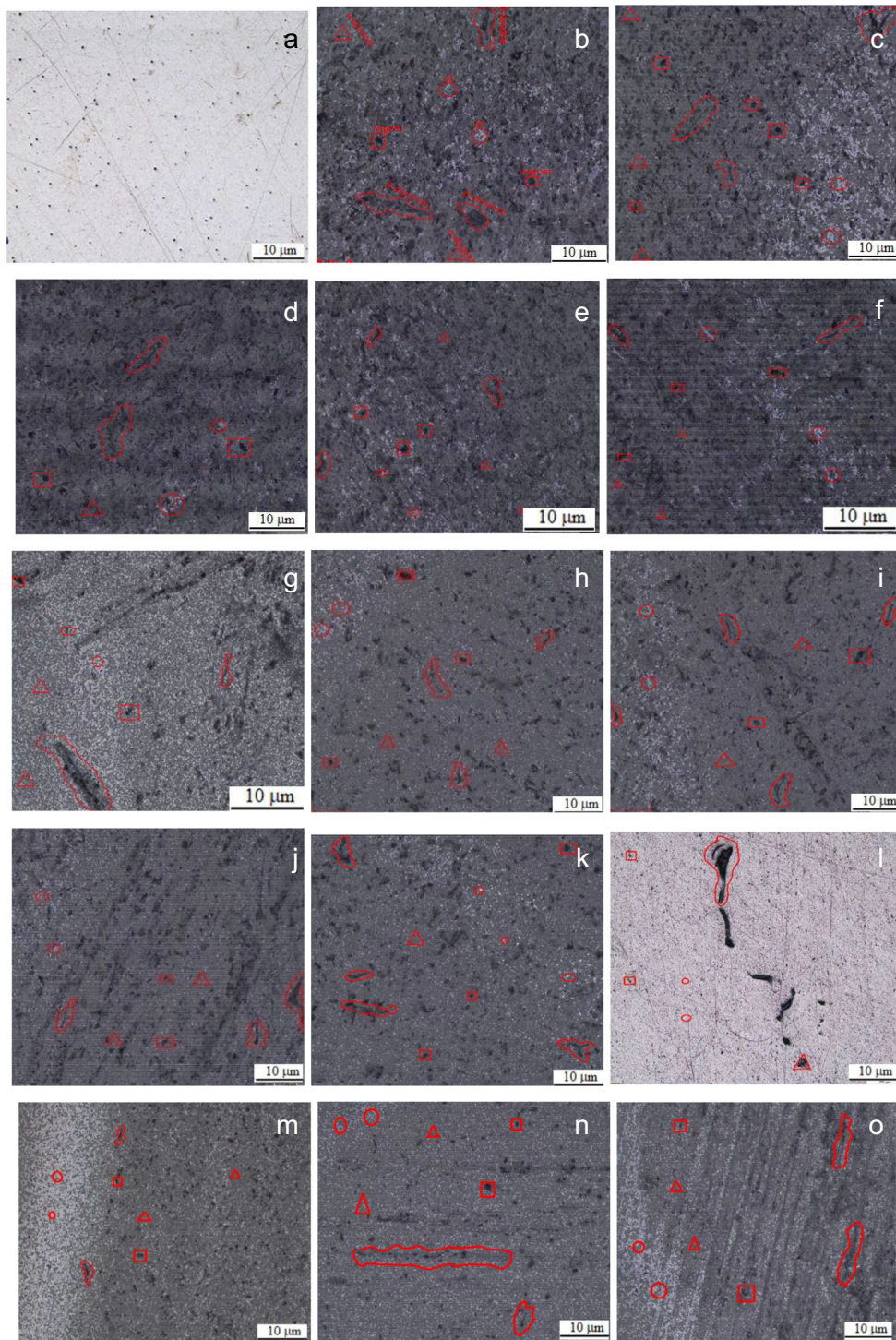
As seen in Fig. 14, the billet temperature increased during forging due to increasing strain energy. While the maximum temperature was stable and stayed under the melting point for the steel, it may exceed the melting point for AA6082 that causes incomplete die filling. The graphs show the solutions at the last substep of the last step on the whole body.

While AA6082 alloy has the highest forgeability at 400 °C, it was 1250 °C for the steel as seen in Fig. 15. The graphs show the solutions at the last substep of the last step on the scoped point. The fact that the deformation capability decreases for AA6082 as the temperature increases is due to incomplete die filling because of the liquid flow of the melted material. Considering the difference in the temperature and the specific heat capacity, which is 950 J/kg·°K for aluminum and 480 J/kg·°K for steels [41], a 39.01% saving in energy per part can be achieved by replacing with AA6082.

As seen in Fig. 16, the residual stress remained in the forged part was lower in AA6082. It means that the part to be produced from aluminum alloy does not need an additional heat treatment for stress relief after the hot forging. The stress decreases at elevated temperatures for both materials. The maximum stress was scoped to determine the forging load. The press force required for hot forging of AA6082 alloy was also less as seen in Fig. 17. This affects the

**Table 4** Calculations from the jump peaks at room temperature

No.	$\sigma_1$ (MPa)	$\sigma_j$ (MPa)	$\dot{\epsilon}_1$ (s <sup>-1</sup> )	$\dot{\epsilon}_2$ (s <sup>-1</sup> )	$m_j = \left(\frac{\ln \sigma_j}{\ln \sigma_1}\right) / \left(\frac{\ln \dot{\epsilon}_2}{\ln \dot{\epsilon}_1}\right)$
1	53.040	54.860	0.000030	3.33E-05	0.320
2	59.160	60.430	0.000100	0.000103	0.648
3	65.380	70.430	0.000160	0.000183	0.547
4	70.520	71.060	0.000227	0.000230	0.523
5	75.090	76.140	0.000283	0.000290	0.597
6	78.680	80.125	0.000347	0.000357	0.640



**Fig. 12** Optic examinations **a** AA6082-O; **b** water quenched, 2 h aged at 175°C; **c** water quenched, 4 h aged at 175°C; **d** water quenched, 8 h aged at 175°C; **e** water quenched, 10 h aged at 175°C; **f** water + 50% polymer mix quenched, 10 h aged at 175°C; **h** water quenched, 2 h aged at 185°C; **i** water quenched, 4 h aged at 185°C; **j** water quenched, 6 h aged at 185°C; **k** water quenched, 8 h aged at 185°C; **l** water quenched, 10 h aged at 185°C; **m** water + 50% polymer mix quenched, 10 h aged at 185°C; **n**

water quenched, 2 h aged at 195°C; **o** water quenched, 4 h aged at 195°C; **p** water quenched, 6 h aged at 195°C; **q** water quenched, 8 h aged at 195°C; **r** water quenched, 10 h aged at 195°C; **s** water + 50% polymer mix quenched, 6 h aged at 195°C; **t** water + 50% polymer mix quenched, 2 h aged at 175°C; **u** water + 50% polymer mix quenched, 4 h aged at 185°C; **v** water + 50% polymer mix quenched, 6 h aged at 195°C; **y** water + 50% polymer mix quenched, 10 h aged at 220°C

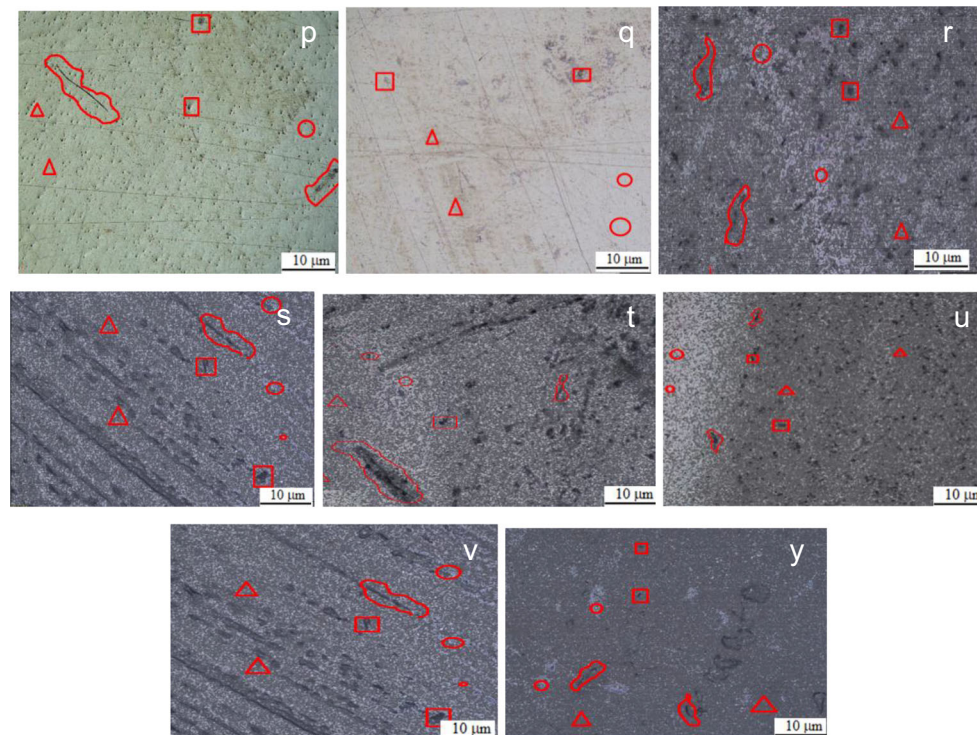


Fig. 12 continued.

competitiveness of the rod end manufacturers by reducing the operating and manufacturing costs.

### 3.5 Fatigue simulation

For the fatigue simulations, Ansys© software is used [26, 42]. Figure 18 shows the safety factor, yield stress, service life, and the biaxial stress distribution results of the rod end loaded to service conditions. As can be deduced from the safety factor solutions, the thinner section was the most sensitive to fatigue. The lowest safety factor was 5.34 for AISI1045, while it was 1.94 for the AA6082 sample 18. The entire part has a sufficient fatigue and static stress capacity for infinite life. Thus the replacement of AISI1045 with AA6082 may be possible without sacrificing the fatigue requirements.








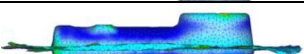
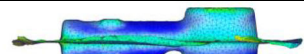


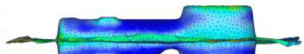
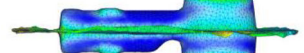

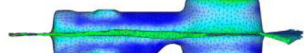
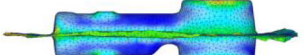
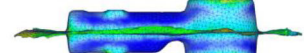
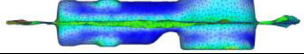
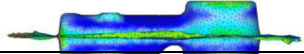
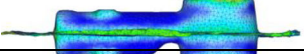
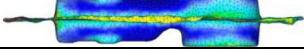
From the biaxial stress solution, it can be seen that normal and shear stresses were present at the body surface. Equivalent von Mises stress distribution is given in Fig. 19. While the maximum equivalent stress was 41.264 MPa for AISI1045, it was 44.38 MPa for AA6082.

For a manufacturer in the competitive world, it is quite important to replace a structural part with the lighter one without sacrificing safety, manufacturing time, and low cost. It is a challenge to replace the material of the forged rod end part that has necessary geometric tolerances and defect-free surfaces. It means that all vehicles having the transmission will be lightened.






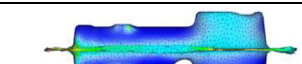
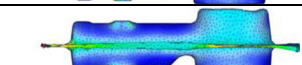
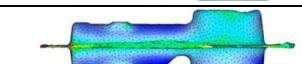
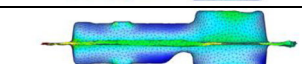
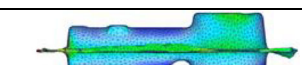
Summarizing the whole results above, the most important contributions of this study are that the aged AA6082 sample was improved significantly in strength as explained by Kvackaj et al. [2].  $\beta$  phases playing important role in the strengthening have a finer distribution in the microstructure up to 4 h of aging [17]. The optimum forging temperature is between 300 and 450 °C which is lower than that of AISI1045 [10]. Increased hardness provides more wear resistance. The fatigue life is more than a million cycles with 1.94 safety factor which is higher than 1.5, as a rule of thumb [31]. Although fatigue and tensile strength appear to be lowered, it still meets the specification requirements [43, 44]. The increased hardness and the fatigue life increase the damage tolerance similar to Al-Li-based alloys [45] which are another alloys used in the aerospace and automotive industry. Due to its higher energy absorption capability, AA6082 would be a good replacement for applications where shock and vibrational loads arise.

In this study, the mechanical tests were performed to identify plasticity model parameters, and the processes were simulated. The strengthening and hardening behaviors were exposed by microstructural investigations. For the validation, hot forging experiments were performed. Results proved that the artificial aged AA6082 could be used for a replacement of the AISI1045 rod end without changing the part design and the manufacturing process. The critical point is that the lower temperature requirement

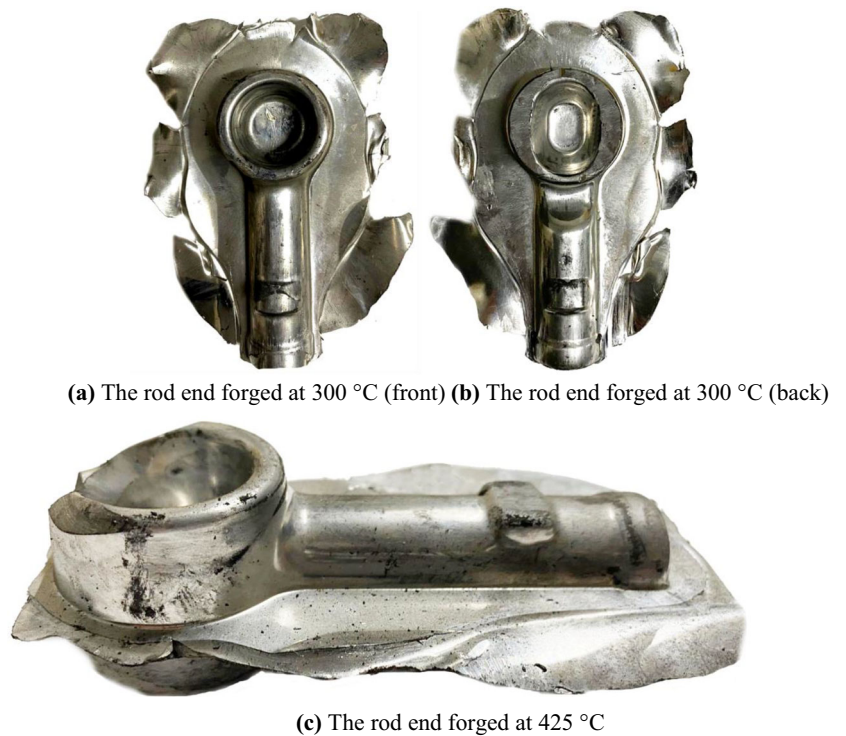
**Table 5** Hot forging simulation results of AISI1045

<b>Initial temp. (°C)</b>	<b>Peak temp. (°C)</b>	<b>Press force (tons)</b>	<b>Die filling (%)</b>	<b>Burr (%)</b>
750	1320	1770	 100	5.37
775	1340	1940	 100	5.54
800	1350	1700	 100	5.55
825	1330	1540	 100	5.47
850	1320	1770	 100	5.49
875	1310	1630	 100	5.52
900	1330	1580	 100	5.55
925	1350	1560	 100	5.55
950	1330	1550	 100	5.64
975	1320	1500	 100	5.52
1000	1340	1400	 100	5.60
1025	1350	1090	 100	5.55
1050	1290	872	 100	5.37
1075	1290	1010	 100	5.49
1100	1290	902	 100	5.64
1125	1280	876	 100	5.4
1150	1360	1000	 100	5.47
1175	1330	715	 100	5.40
1200	1350	727	 100	5.64
1225	1370	801	 100	5.55
1250	1360	715	 100	5.52

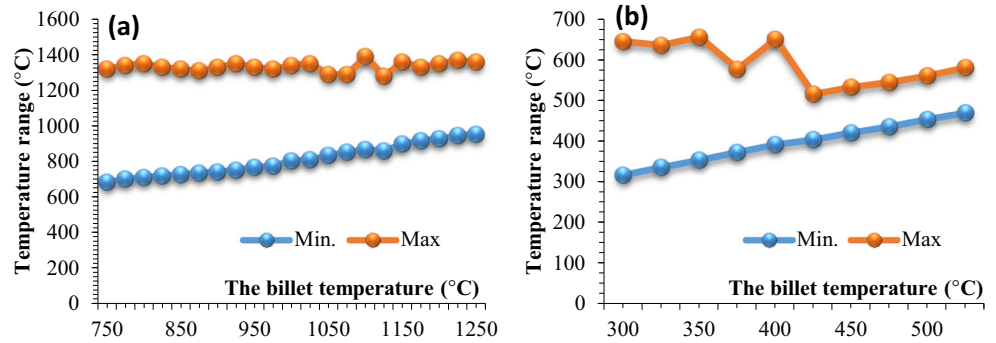
**Table 6** Hot forging simulation results of AA6082

Initial temp. (°C)	Peak temp. (°C)	Press force (tons)	Die filling (%)	Burr (%)
300	648	413	 100	3.75
325	639	437	 100	4.13
350	660	397	 100	4.11
375	577	311	 100	4.15
400	651	353	 98	4.12
425	516	155	 94	5.11
450	651	353	 94	5.17
475	516	153	 93	4.93
500	561	145	 93	4.97
525	581	140	 92	5.07

**Fig. 13** The hot forged AA6082 rod ends. **a** The rod end forged at 300 °C (front). **b** The rod end forged at 300 °C (back). **c** The rod end forged at 425 °C



**Fig. 14** The billet temperature ranges during the hot forging of a AISI1045 and b AA6082



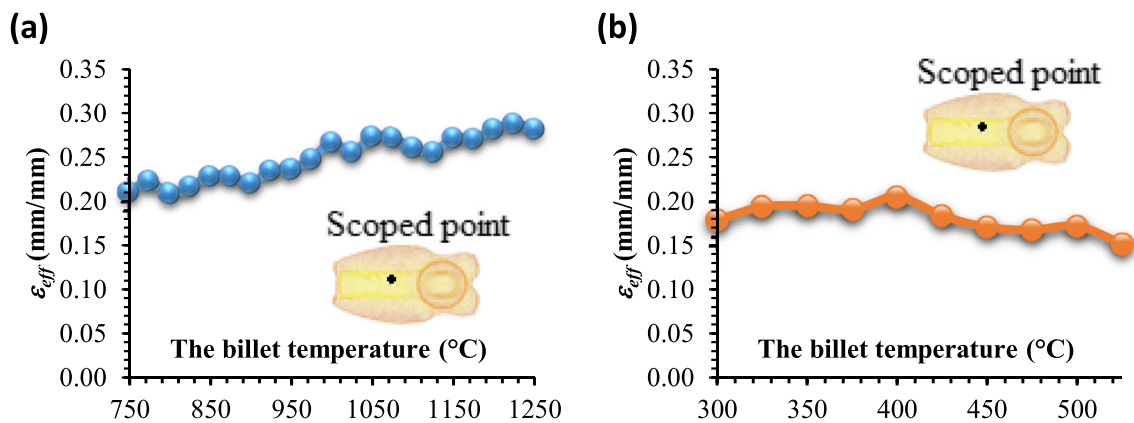
leads to the more economical forging process. Hence, it becomes a cheaper alternative among other aluminum alloys. Therefore, it makes the alloy most important for the forged part manufacturers.

**4 Conclusions**

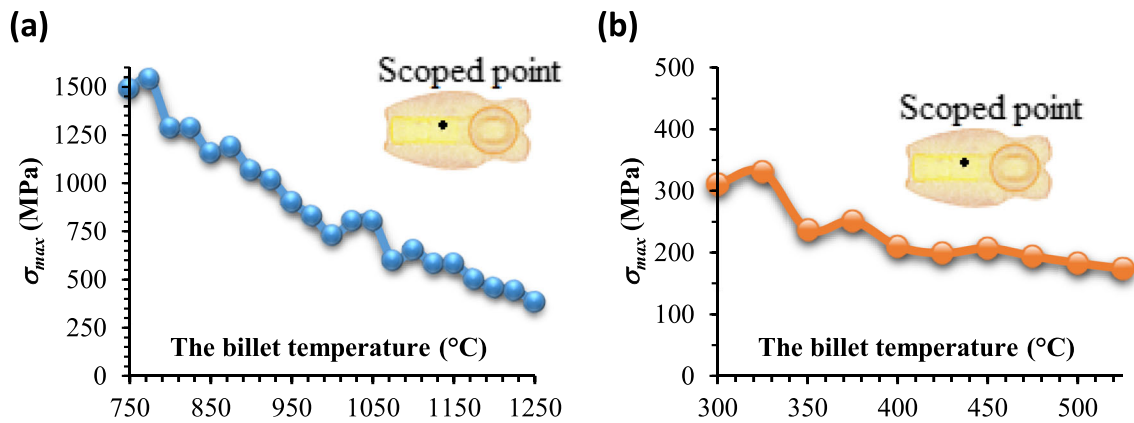
In this study, a possible replacement of AISI1045 with AA6082 was investigated for an automotive structural part.

The most suitable artificial aging conditions were determined for AA6082. The results were used in the fatigue and hot forging simulations. Microstructural analysis was also performed. The fatigue life of the rod end, the press force requirement for the forging process, the burr ratio, and the processing time have been evaluated. The most important conclusions can be summarized as follows:

- The highest tensile strength of 406 MPa can be achieved by dissolving at 500 °C for 2 h, quenching



**Fig. 15** The effective strain in the hot forging of a AISI1045 and b AA6082



**Fig. 16** The maximum stress in the hot forging of a AISI1045 and b AA6082

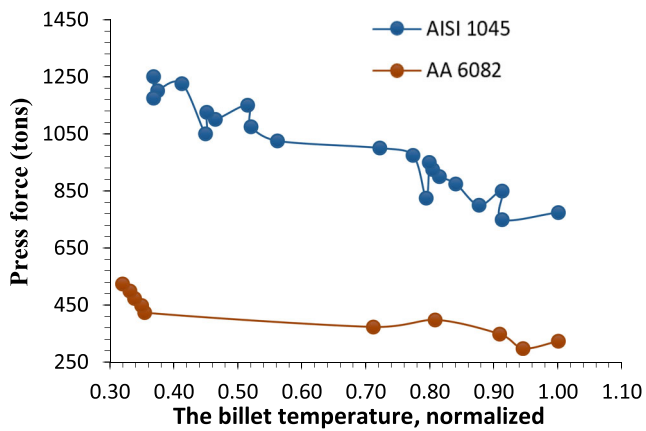


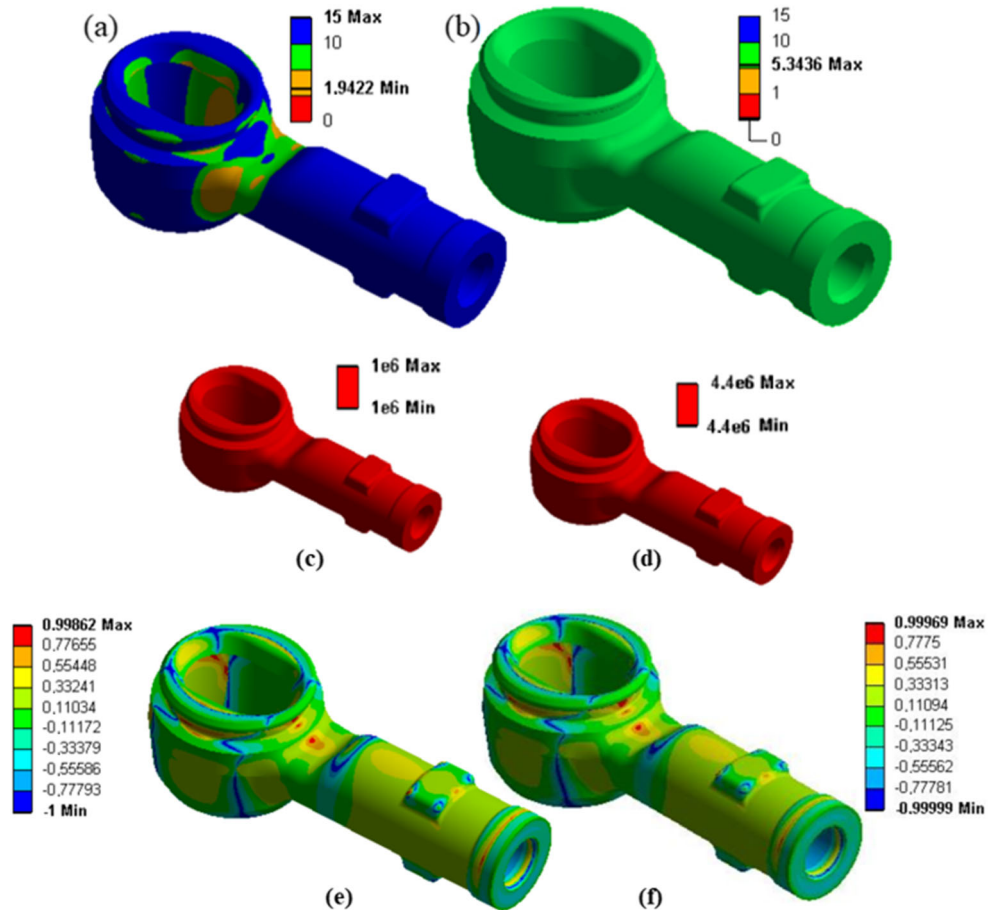
Fig. 17 Press force requirements

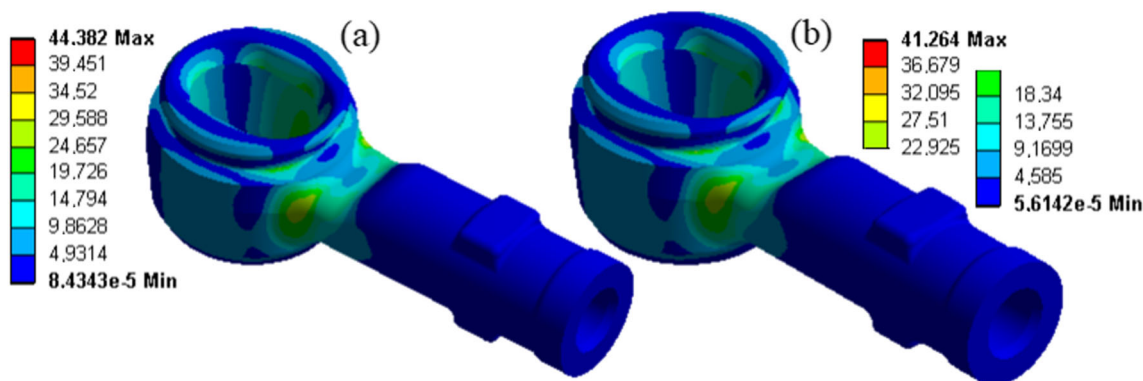
in the air, aging at 185 °C for 4 h, and cooling in the air. Under these circumstances, the AA6082 rod end has at least one million cycles service life. Although increased hardness provides more wear resistance to AA6082, it suffers from energy-absorbing capability.

- Aged AA6082’s cold forgeability is poor due to brittle nature of the material and crack initiations. Thus, warm or hot forging is recommended.

- For warm forging of the AA6082, it is recommended to maintain temperature ranges of 160–300 °C for a good microstructure, strength, and forging energy absorption capability.
- For hot forging of the AA6082, more than 425 °C billet temperature is not suitable. Because the local material melting during process causes incomplete die filling. It is concluded that the hot forging up to 425 °C is suitable.
- Due to its higher energy-absorbing capability, AA6082 would be a good replacement for applications where shock and vibrational loads arise.
- $\beta$  phases are the most effective on strengthening of AA6082.  $\beta$  phases have a finer distribution in the microstructure up to 4 h of aging. Longer aging time results in coarser grains and dendrite formation leading to reduced strength.
- Due to less energy consumption during its hot forging, AA6082 guarantees more economical manufacturing without sacrificing service requirements. The rod end part currently manufactured from AISI1045 can be replaced by AA6082 without any design changes.

Fig. 18 Safety factor solutions **a** for AA6082 and **b** for AISI1045. Service life (cycle) **c** for AA6082 and **d** for AISI1045. Biaxiality indication **e** for AA6082 and **f** for AISI1045





**Fig. 19** Stress solutions (MPa) **a** for AA6082 and **b** for AISI1045

**Acknowledgements** The authors would like to thank Niğde Ömer Halisdemir University Scientific Research Projects Unit for the Grant No. FEB 2018/14-BAGEP. We thank Ditaş Yedek Parça İmalat ve Teknik Inc. for their technical support. This study has been produced from the master's thesis accepted by Niğde Ömer Halisdemir University, Graduate School of Natural and Applied Sciences, with confirmation number 30, on August 07, 2020. The authors appreciate the valuable comments from the reviewers.

**Materials availability** n/a

**Code availability** n/a

**Author contribution** All authors have contributed equally.

**Funding** This work was supported by Niğde Ömer Halisdemir University Scientific Research Projects Unit for the Grant No. FEB 2018/14-BAGEP. This study was produced from the master's thesis which was supervised by İlyas Kacar and accepted by Niğde Ömer Halisdemir University, Graduate School of Natural and Applied Sciences, with confirmation number 30, on August 07, 2020.

**Data availability** n/a

## Declarations

**Ethics approval** n/a

**Consent to participate** n/a

**Consent for publication** Yes

**Conflict of interest** The authors declare no competing interests.

## References

- Zvinys J, Kandrotaitė Janutiene R, Meskys J, Juzenas K (2012) Investigation of thermo mechanical effect on structure and properties of aluminium alloy 6082. *Int Virtual J Sci Tech Innov Ind*:3–6
- Kvackaj T, Fujda M, Besterci M (2009) Ultra fine microstructure and properties formation of EN AW 6082 alloy. *Transactions of the Japan Society for Aeronautical and Space Sciences, Space Technology Japan* 7 (ists26):Pc\_85-Pc\_91. [https://doi.org/10.2322/tstj.7.Pc\\_85](https://doi.org/10.2322/tstj.7.Pc_85)
- Prabhukhot A (2015) Effect of heat treatment on hardness and corrosion behavior of 6082-T6 aluminium alloy in artificial Sea water. *International Journal of Materials Science and Engineering* 3:287–294. <https://doi.org/10.17706/ijmse.2015.3.4.287-294>
- Torca I, Aginagalde A, Esnaola JA, Galdos L, Azpilgain Z, Garcia C (2010) Tensile behaviour of 6082 aluminium alloy sheet under different conditions of heat treatment, temperature and strain rate. *Key Eng Mater* 423:105–112. <https://doi.org/10.4028/www.scientific.net/KEM.423.105>
- Bouquerel J, Diawara B, Dubois A, Dubar M, Vogt JB, Najjar D (2015) Investigations of the microstructural response to a cold forging process of the 6082-T6 alloy. *Mater Design* 68:245–258. <https://doi.org/10.1016/j.matdes.2014.12.005>
- Chang Y-L, Hung F-Y, Lui T-S (2019) Study of microstructure and tensile properties of infrared-heat-treated cast-forged 6082 aluminium alloy. *Journal of Materials Research and Technology* 8(1): 173–179. <https://doi.org/10.1016/j.jmrt.2017.10.004>
- Krolo J, Lela B, Ljumović P, Bagavac P (2019) Enhanced mechanical properties of aluminium alloy EN AW 6082 recycled without remelting. *Tehnicki Vjesnik* 26:1253–1259. <https://doi.org/10.17559/TV-20180212160950>
- Kumar N, Jayaganthan R, Brokmeier H-G (2017) Effect of deformation temperature on precipitation, microstructural evolution, mechanical and corrosion behavior of 6082 Al alloy. *T Nonferrous Metal Soc* 27(3):475–492. [https://doi.org/10.1016/S1003-6326\(17\)60055-4](https://doi.org/10.1016/S1003-6326(17)60055-4)
- Gökçil E, Akdi S, Birol Y (2015) A novel processing route for the manufacture of EN AW 6082 forged components. *Mater Res Innov* 19:S10-311. <https://doi.org/10.1179/1432891715Z.0000000002179>
- Birol Y, Ilgaz O, Akdi S, Unuvar E (2014) Comparison of cast and extruded stock for the forging of AA6082 alloy suspension parts. *Adv Mater Res* 939:299–304. <https://doi.org/10.4028/www.scientific.net/AMR.939.299>
- Birol Y, Gökçil E, Akdi S (2017) Potential of twin-belt-cast EN AW 6082 blanks for the manufacture of wishbone suspension forgings. *Int J Adv Manuf Technol* 92:3693–3701. <https://doi.org/10.1007/s00170-017-0446-3>
- Kumar N, Goel S, Rengaswamy J, Brokmeier H-G (2015) Effect of solution treatment on mechanical and corrosion behaviors of 6082-T6 Al alloy. *Metallography, Microstructure and Analysis* 4:411–422. <https://doi.org/10.1007/s13632-015-0219-z>
- Shao Z, Lee J, Wang J, Lin J, Jiang J (2020) A study of various heating effects on the microstructure and mechanical properties of AA6082 using EBSD and CPFE. *J Alloys Compd* 818:152921. <https://doi.org/10.1016/j.jallcom.2019.152921>



14. Sürmen Ö, Tarakçı M, Gencer Y, Zeytin S Improvement of heat treatment application of aluminium forged parts. In: IMMC 2016, 18th International Metallurgy & Materials Congress, 2016. UCTEA Chamber of Metallurgical & Materials Engineers, pp 721–724
15. Mrówka-Nowotnik G, Sieniawski J (2005) Influence of heat treatment on the microstructure and mechanical properties of 6005 and 6082 aluminium alloys. *J Mater Process Technol* 162–163:367–372. <https://doi.org/10.1016/j.jmatprotec.2005.02.115>
16. Österreicher J, Kumar M, Schiffel A, Schwarz S, Hillebrand D, Bourret G (2016) Sample preparation methods for scanning electron microscopy of homogenized Al-Mg-Si billets: a comparative study. *Mater Charact*:122. <https://doi.org/10.1016/j.matchar.2016.10.020>
17. Yibo P, Gang W, Tianxing Z, Shangfeng P, Yiming R (2013) Dynamic mechanical behaviors of 6082-T6 aluminum alloy. *Adv Mech Eng* 5:878016. <https://doi.org/10.1155/2013/878016>
18. Kumar M, Baloch M, Abro MI, Memon S, Chandio A (2019) Effect of artificial aging temperature on mechanical properties of 6061 aluminum alloy. *Mehran University Research Journal of Engineering and Technology* 38:31–36. <https://doi.org/10.22581/muet1982.1901.03>
19. Xu Z, Ma H, Zhao N, Hu Z (2020) Investigation on compressive formability and microstructure evolution of 6082-T6 aluminum alloy. *Metals-Basel* 10:469. <https://doi.org/10.3390/met10040469>
20. Cabibbo M, Evangelista E, Vedani M (2005) Influence of severe plastic deformations on secondary phase precipitation in a 6082 Al-Mg-Si alloy. *Metallurgical and Materials Transactions A: Physical Metallurgy and Materials Science* 36:1353–1364. <https://doi.org/10.1007/s11661-005-0226-9>
21. Ben Naser T, Bobor K, Krallics G (2014) Tensile behavior of multiple forged 6082 Al alloy. *Periodica Polytechnica Mechanical Engineering* 58. <https://doi.org/10.3311/PPme.7275>
22. ASTM (2002) Standard test methods of tension testing wrought and cast aluminum- and magnesium-alloy products. vol ASTM B 557M – 02a. ASTM International, West Conshohocken, PA 19428-2959, United States
23. ASTM (2004) Standard practice for strain-controlled fatigue testing. vol ASTM E 606 – 92. ASTM International, West Conshohocken, PA 19428-2959, United States
24. ISO (2016) Metallic materials — Charpy pendulum impact test — Part 1: Test method. vol ISO 148-1:2016. International Organization for Standardization, Geneva, Switzerland
25. ASTM (2017) Standard test methods for Vickers hardness and knoop hardness of metallic materials. vol ASTM E 92. ASTM International, West Conshohocken, PA 19428-2959, United States
26. Inc. D (2020) Hot forging press workshop Ditas Academia
27. Tunc O (2020) Investigation on forging performance of AA6082. Niğde Omer Halisdemir University, Niğde, MSc.
28. SFTC (2020) DEFORM V12.0.2 user's manual. Scientific Forming Technologies Corporation, Columbus, Ohio
29. Ludwik P (1909) *Elemente der Technologischen Mechanik*. Springer-Verlag Berlin Heidelberg. <https://doi.org/10.1007/978-3-662-40293-1>
30. Mises RV (1928) *Mechanik der plastischen Formänderung von Kristallen*. ZAMM - Journal of Applied Mathematics and Mechanics / Zeitschrift für Angewandte Mathematik und Mechanik 8(3):161–185. <https://doi.org/10.1002/zamm.19280080302>
31. Budynas R, Nisbett K (2010) *Shigley's mechanical engineering design*. McGraw-Hill Education,
32. Al-Rubaie KS, Del Grande MA, Travessa DN, Cardoso KR (2007) Effect of pre-strain on the fatigue life of 7050-T7451 aluminium alloy. *Mater Sci Eng A* 464(1):141–150. <https://doi.org/10.1016/j.msea.2007.02.024>
33. Kilic S, Kacar I, Sahin M, Ozturk F, Erdem O (2019) Effects of aging temperature, time, and Pre-strain on mechanical properties of AA7075. *Mater Res* 22
34. Thangarasu A, Murugan N, Dinaharan I (2014) Production and wear characterization of AA6082 -TiC surface composites by friction stir processing. *Procedia Engineering* 97:590–597. <https://doi.org/10.1016/j.proeng.2014.12.287>
35. Werber A, Liewald M (2012) Influence of pre-strain and heat treatment on mechanical properties of aluminum sheet. *Int J Mater Form* 5(4):307–315. <https://doi.org/10.1007/s12289-011-1051-x>
36. Ozturk F, Toros S, Kilic S (2010) Tensile deformation behavior of AA5083-H111 at cold and warm temperatures. *Int J Mater Res* 101(9):1172–1179. <https://doi.org/10.3139/146.110391>
37. Kılıç S (2016) *Twip Çeliklerde İkizlenme Mekanizmasının Mekanik Özelliklere Etkisinin İncelenmesi*. Niğde University, Niğde
38. Kilic S, Ozturk F, Picu CR (2018) Investigation of the performance of flow models for TWIP steel. *J Mater Eng Perform* 27(8):4364–4371. <https://doi.org/10.1007/s11665-018-3504-6>
39. Zulfi FR, Korda AA (2016) Effect of pre-strain on mechanical properties and deformation induced transformation of 304 stainless steel. *J Phys Conf Ser* 739:012039. <https://doi.org/10.1088/1742-6596/739/1/012039>
40. Kacar İ, Kılıç S (2018) *Hardening rules*. In: Güngör T, Kılıç GB, Uyumaz A, Görgülü ÜS (eds) *Innovative approaches in engineering*. Gece Kitaplığı, Ankara, Turkey, pp 175–194
41. Çengel YA (1998) *Heat transfer: a practical approach*. WBC McGraw-Hill,
42. Ansys (2004) *Theory Manual Version 9.0*. vol v11. ANSYS Inc., Canonsburg, PA, USA.
43. Szulc M, Malujda I, Talaška K (2016) Method of determination of safety factor on example of selected structure. *Procedia Engineering* 136:50–55. <https://doi.org/10.1016/j.proeng.2016.01.173>
44. Poutanen T, Lämsivaara T, Pursiainen S, Mäkinen J, Asp O (2021) Calculation of safety factors of the eurocodes. *Appl Sci* 11:208. <https://doi.org/10.3390/app11010208>
45. Kilic S, Kacar I, Ozturk F (2019) New trend in aerospace industry: Al-Li based alloys. *J Fac Eng Archit Gaz* 34(1):275–296

**Publisher's note** Springer Nature remains neutral with regard to jurisdictional claims in published maps and institutional affiliations.